Original Article | Gastrointestinal Imaging

http://dx.doi.org/10.3348/kjr.2014.15.2.226
pISSN 1229-6929 · eISSN 2005-8330
Korean J Radiol 2014;15(2):226-234

Korean Journal of Radiology
KJR

Differentiating between Adenomyomatosis and Gallbladder Cancer: Revisiting a Comparative Study of High-Resolution Ultrasound, Multidetector CT, and MR Imaging

Sang Heum Bang, MD, Jae Young Lee, MD, Hyunsik Woo, MD, Ijin Joo, MD, Eun Sun Lee, MD, Joon Koo Han, MD, Byung Ihn Choi, MD

All authors: Department of Radiology and the Institute of Radiation Medicine, Seoul National University Hospital, Seoul 110-744, Korea

Objective: To compare the diagnostic performance of high-resolution ultrasound (HRUS) with contrast-enhanced CT and contrast-enhanced magnetic resonance imaging (MRI) with MR cholangiopancreatography (MRCP) to differentiate between adenomyomatosis (ADM) and gallbladder cancer (GBCA).

Materials and Methods: Forty patients with surgically proven ADM (n = 13) or GBCA at stage T2 or lower (n = 27) who previously underwent preoperative HRUS, contrast-enhanced CT, and contrast-enhanced MRI with MRCP were retrospectively included in this study. According to the well-known diagnostic criteria, two reviewers independently analyzed the images from each modality separately with a five-point confidence scale. The interobserver agreement was calculated using weighted κ statistics. A receiver operating characteristic curve analysis was performed and the sensitivity, specificity, and accuracy were calculated for each modality when scores of 1 or 2 indicated ADM.

Results: The interobserver agreement between the two reviewers was good to excellent. The mean Az values for HRUS, multidetector CT (MDCT), and MRI were 0.959, 0.898, and 0.935, respectively, without any statistically significant differences between any of the modalities ($p > 0.05$). The mean sensitivity of MRI with MRCP (80.8%) was significantly higher than that of MDCT (50.0%) ($p = 0.0215$). However, the mean sensitivity of MRI with MRCP (80.8%) was not significantly different from that of HRUS (73.1%) ($p > 0.05$). The mean specificities and accuracies among the three modalities were not significantly different ($p > 0.05$).

Conclusion: High-resolution ultrasound and MRI with MRCP have comparable sensitivity and accuracy and MDCT has the lowest sensitivity and accuracy for the differentiation of ADM and GBCA.

Index terms: *Gallbladder; Adenomyomatosis; Gallbladder cancer; High-resolution ultrasound; CT; MRI*

INTRODUCTION

Adenomyomatosis (ADM) of the gallbladder (GB) is a relatively common disease with an incidence of 2–5% among specimens obtained from patients at cholecystectomy (1-4). It is pathologically defined as an epithelial proliferation and hypertrophy of the GB muscularis with an outpouching of the mucosa into the thickened muscular layer (Rokitansky-Aschoff sinus) (2, 4). Three morphologic types of ADM of the GB are known; diffuse, segmental and fundal (1-4). The differentiation from GB cancer is still required because of the similarity in the appearance between ADM and GB

Received February 6, 2013; accepted after revision December 19, 2013.
This study was supported by the R&D program of MKE/KEIT (10033726, Ultrasound Multi-harmonic Imaging Techniques).
Corresponding author: Jae Young Lee, MD, Department of Radiology, Seoul National University Hospital, 101 Daehak-ro, Jongno-gu, Seoul 110-744, Korea.
• Tel: (822) 2072-3073 • Fax: (822) 743-6385
• E-mail: leejy4u@snu.ac.kr

Korean Journal of Radiology
KJR

cancer, although many studies have reported imaging findings of ADM of the GB using ultrasound (US), computed tomography (CT), and magnetic resonance imaging (MRI) (5, 6).

According to a report published in 2001, conventional US was inferior to helical CT and MRI with the half-Fourier rapid acquisition with relaxation enhancement (RARE) technique for the differentiation of ADM and GB cancer (7). However, there have been striking developments in the US imaging technology since the beginning of the 2000s. These technological developments include harmonics, compounding techniques and speckle reduction imaging. These techniques are well known to significantly enhance contrast and spatial resolution and reduce artifacts and noise (8-10) and are all available in low-MHz convex and high-MHz linear transducers. Also the use of higher MHz is helpful for the further enhancement of the spatial resolution.

Recently, the concurrent use of these advanced techniques and high-MHz imaging (high-resolution US, HRUS) was reported as more useful for the differentiation between ADM and GB cancer than the conventional US because the combination is better to demonstrate intramural cysts and echogenic areas within the thickened GB wall (11). However, to the best of our knowledge, no published studies have compared the diagnostic performance of HRUS with that of CT and MRI for differentiating ADM and GB cancer yet. Therefore, the purpose of this study was to compare the diagnostic performance of HRUS with contrast-enhanced CT and contrast-enhanced MRI with MR cholangiopancreatography (MRCP) for the differentiation of ADM and GB cancer.

MATERIALS AND METHODS

Patients

This study was approved by our institutional review board and an informed consent was not required. Between January 2006 and January 2012 a total of 3133 patients underwent preoperative HRUS and subsequent a cholecystectomy. Among them, 168 patients underwent within 3 month HRUS, contrast-enhanced CT and contrast-enhanced MRI with MRCP due to GB diseases. Among the 168 patients, for 40 patients either ADM (n = 13) or gallbladder cancer at stage T2 or lower without lymph node or distant metastasis (n = 27) was pathologically confirmed. Only subjects with GB cancers at stage T2 or lower without lymph node or distant metastasis were included because this type of GB cancer is the principle type where the differentiation from ADM is difficult.

The ADM group (n = 13) consisted of 5 males and 8 females with a mean age of 61.8 years (range, 34–84 years). The group included two patients with a generalized involvement of the GB wall, four with segmental involvement and seven with a fundal involvement. The indications for the surgery of a ADM were either a symptomatic ADM (n = 5) or difficulties in the differentiation between ADM and GB cancer by imaging findings (n = 8). The GB cancer group (n = 27) consisted of 13 males and 14 females with a mean age of 65 years (range, 52–82 years). Four patients presented T1a tumors, two presented T1b tumors, and the remaining 21 presented T2 tumors with respect to the T staging. In the GB cancer group were included two patients with the wall-thickening type, 19 with the polypoid type, one with the lumen-replacing type and five with a combination of the wall-thickening and polypoid types.

Imaging

HRUS

All patients underwent transabdominal HRUS using a LOGIQ 9 scanner (GE Healthcare, Milwaukee, WI, USA) performed by two abdominal radiologists with more than 10 years of experience in abdominal US. The US examination process is described below. First, the GB was examined by the intercostal and/or subcostal approach using a convex probe (4C, bandwidth 1.5–4.5 MHz) with real-time spatial compound imaging techniques (3 compound beams per scanning frame), a mild degree of speckle reduction techniques and harmonic imaging techniques.

Then, the GB was evaluated using a linear probe (7L, bandwidth 2.5–7.0 MHz). To exactly evaluate the GB with the linear probe, real-time spatial compound imaging techniques (3 and 5 compound beams per scanning frame) and a mild degree of speckle reduction techniques with or without harmonic imaging techniques were used. In 34 of the 40 patients (8 with ADM and 26 with cancer color Doppler studies were used) to visualize color Doppler twinkling artifacts or to demonstrate the vascularity of the lesion. In six patients (five with ADM and one with GB cancer), color Doppler studies were not available.

Contrast-Enhanced CT

Various multidetector CT (MDCT) scanners were used,

including in 10 patients the Brilliance 64 (64 channels, Philips Healthcare, Cleveland, OH, USA); in 8 patients the Somatom Definition (64 channels, Siemens Medical Solutions, Forchheim, Germany); in 18 patients the Sensation 16 (16 channels, Siemens Medical Solutions, Forchheim, Germany) and in 4 patients the LightSpeed Ultra (8 channels, GE Healthcare, Milwaukee, WI, USA). The arterial and portal venous phases were obtained in 36 patients after the injection of 120 mL of nonionic contrast material (iopromide, Ultravist 370, Bayer Schering Pharma) through an 18-gauge angiographic catheter at a of 3–4 mL/s rate administered with an automatic power injector. In 4 patients was the portal venous phase obtained alone.

The scanning parameters for the MDCT scanners were as follows: a gantry rotation time of 0.5–0.75 seconds; 4 x 2.5 mm, 8 x 1.25 mm, 16 x 0.75 mm or 64 x 0.625 mm detector configuration; 2.5–3.2 mm slice thickness; pitch of 0.891–1.75; 3-mm reconstruction interval for each phase; 150–200 mAs; 120 kVp; and a 512 x 512 matrix. Coronal and sagittal multiplanar reformation images with a 3-mm reconstruction interval were made by an expert technician. The scan delay for the arterial phase was 15–19 seconds after the achievement of 100-Hounsfield unit attenuation of the descending aorta measured with a bolus-tracking technique (12). A 30- to 33-second scan delay after the arterial phase acquisition was used for the portal venous phase acquisition.

Contrast-Enhanced MRI with MRCP

All MRI was performed on a 3-T superconducting system (Verio, Siemens Medical Solutions, Erlangen, Germany, n = 19) and on a 1.5-T superconducting system (Signa Excite HDX, GE Medical Systems, Milwaukee, WI, USA, n = 19; Sonata, Siemens Healthcare, or Magnetom Vision, Siemens Healthcare, Berlin, Germany, n = 6) with a phased-array torso coil.

All patients underwent contrast-enhanced MRI including MRCP. The MRI sequence consisted of baseline images and contrast-enhanced dynamic images. For baseline MR images were performed a T2-weighted single-shot fast spin-echo or half-Fourier acquisition single-shot turbo spin-echo (HASTE) sequence (repetition time [TR]/echo time [TE], 700–982/92–102; flip angle, 90–150°; echo-train length, 1 [1.5T SignaExite] or 256; matrix size, 320–384 x 256–307; slice thickness, 7 mm), breath-hold T1-weighted gradient-recalled echo in-phase (TR/TE 4–170/2.3–5.0; flip angle, 9–70°; echo-train length, 1; matrix size, 256–320 x 167–285; slice thickness, 7 mm) and out-of-phase (TR/TE 4–170/1.3–2.4; flip angle, 9–70°; matrix size, 256–320 x 167–285; slice thickness, 7 mm) sequences. The field of view was 320–380 mm and was adjusted according to the patient size.

Magnetic resonance cholangiopancreatography examinations were obtained with a thick-slab, T2-weighted fast spin-echo sequence (TR/TE 2500–4000/909–1100; flip angle, 90–180°; echo-train length, 1 [1.5T SignaExite] or 256; matrix size, 256–384 x 240–256; slab thickness, 60 mm) and thin-slab multisection HASTE sequence (TR/TE 2000–4000/545–1082.8; flip angle, 90–180°; echo-train length, 1 [1.5T SignaExite] or 105; matrix size, 320–384 x 314–366; slab thickness, 1–2 mm) in the coronal plane. At least five thick-slab, T2-weighted fast spin-echo MRCP images were obtained with coronal and ± 15° and ± 30° oblique coronal angles. Thin-slab, 3-D, T2-weighted array spatial sensitivity-encoding technique MRCP images were obtained by the acquisition of 15 sections per breath-hold (volume of coverage, 60 mm^3).

After the acquisition of the baseline MRI and MRCP images, multiphasic dynamic images composed of the arterial, portal and equilibrium phases were obtained with a chemically selective, fat-suppressed spoiled 3-D gradient-recalled echo MR sequence after an IV injection of 0.1 mmol/kg gadobenate dimeglumine (MultiHance, Bracco SpA, Milan, Italy) at an injection rate of 2 mL/s. After the contrast administration, the arterial, portal and equilibrium phase images were obtained at 20–35 seconds, 45–60 seconds and 3 minutes, respectively. The imaging parameters of the fat-suppressed, 3-D gradient-recalled echo sequence were as follows: TR/TE 3.4–4.9/1.2–2.3; flip angle, 10–12°; matrix size, 320–384 x 179–307 with a three-fourths rectangular field of view; array spatial sensitivity-encoding technique with an acceleration factor of 2; number of signals acquired, 1; and 36–40 partitions interpolated to 72–80 for an effective slice thickness of 2.8–5.0 mm. All images were obtained in the transverse plane and an additional coronal image was obtained after the acquisition of the portal phase image.

Image Analysis

The patient informations on the images were removed and the HRUS, CT, and MRI with MRCP images were separated and randomly assigned to two experienced abdominal radiologists with 17 and 8 years of experience in abdominal radiology regardless of the imaging type. To avoid recall

Korean Journal of Radiology
KJR

bias, all included images were independently reviewed on a Picture Archiving Communication System workstation monitor (m-view; Infinitt, Seoul, Korea), 4 months after last study had been performed. The radiologists were blinded to the radiology report and histopathologic diagnosis. However, they were aware of the study's purpose to differentiate between ADM and GB cancer.

Diagnostic criteria for ADM on HRUS were as follows: the definite presence of intramural cysts indicating Rokitansky-Aschoff sinuses; intramural echogenic spots, representing intramural calcification; or cholesterol deposits in the Rokitansky-Aschoff sinuses (13-17). Diagnostic criteria for ADM on CT were as follows: the presence of the Rosary sign (enhancing mucosal epithelium with intramural diverticula surrounded by the relatively unenhanced, hypertrophied GB muscle coat), multiple intramural cysts or discrete hypoattenuating lesions (16, 18-20). The only diagnostic criterion for ADM on MRI was the presence of multiple intramural cysts in the thickened wall (pearl necklace sign) (21-23). On the other hand, the diagnostic criteria for GB cancer with a stage T2 or lower on HRUS, CT, and MRI were as follows: focal or diffuse mural wall thickening with a mucosal lesion and an intraluminal polypoid mass lacking the pathognomonic findings of ADM as described above (24). Typical imaging findings for ADM and GB cancer for each modality, including HRUS, CT, and MRI with MRCP, are shown in Figures 1 and 2.

The reviewers scored each set of images on a five-point confidence scale based on the following criteria: 1) definite ADM (definite presence of pathognomonic signs for ADM), 2) probable ADM (probable presence of pathognomonic signs for ADM), 3) indeterminate (thickened GB wall without evidence favoring ADM or cancer), 4) probable cancer (thickened GB wall with the probable presence of a mucosal lesion and the absence of pathognomonic signs for ADM), and 5) definite cancer (thickened GB wall with the definite presence of a mucosal lesion and the absence of pathognomonic signs for ADM).

Statistical Analysis

The two reviewers evaluated the diagnostic performance of each modality in terms of the differentiation between ADM and GB cancer with a receiver operating characteristic (ROC) curve analysis. To determine the diagnostic accuracy of each modality for the two reviewers, the area under the ROC curve (Az) value was evaluated. Factors with Az values greater than 0.80 were regarded as good diagnostic accuracy (25). The Az values of each imaging modality acquired from the ROC curves were statistically compared using the paired Z-test. The presence of ADM was regarded as a score of 1 or 2 (probable or definite ADM of the GB). Also the mean sensitivity, specificity and accuracy of each imaging modality for the diagnosis of ADM were assessed using the McNemar test with a Bonferroni correction. The degree of interobserver agreement was considered with weighted κ statistics and was interpreted as follows: poor agreement, less than 0.40; fair to good agreement, 0.40–0.75; and excellent agreement, 0.75 or greater. All statistical analyses were performed with commercially available statistical software (Medcalc, version 11.5.1, Mariakerke, Belgium).

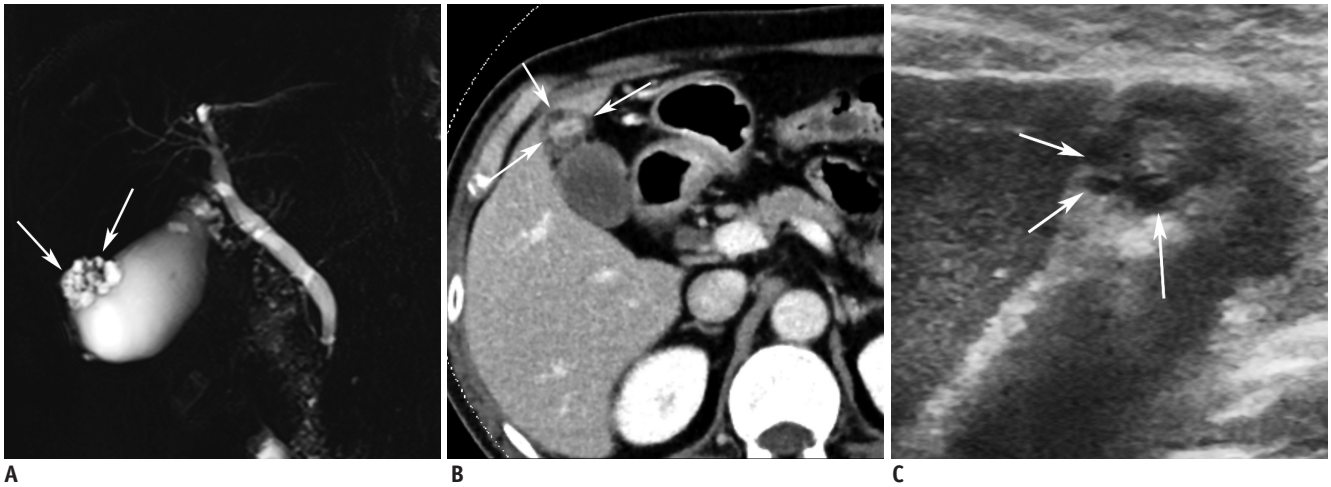

Fig. 1. Fundal adenomyoma of gallbladder in 62-year-old male.
A. MR image with thick-slab, T2-weighted fast spin-echo sequence shows typical "pearl necklace sign" at fundus of gallbladder (arrows). **B.** CT image during portal venous phase demonstrates fundal abnormality with enhancing epithelium and multiple intramural cystic lesions (Rosary sign) (arrows). **C.** High resolution ultrasound image showing multiple intramural cysts (arrows) within thickened wall at fundus.

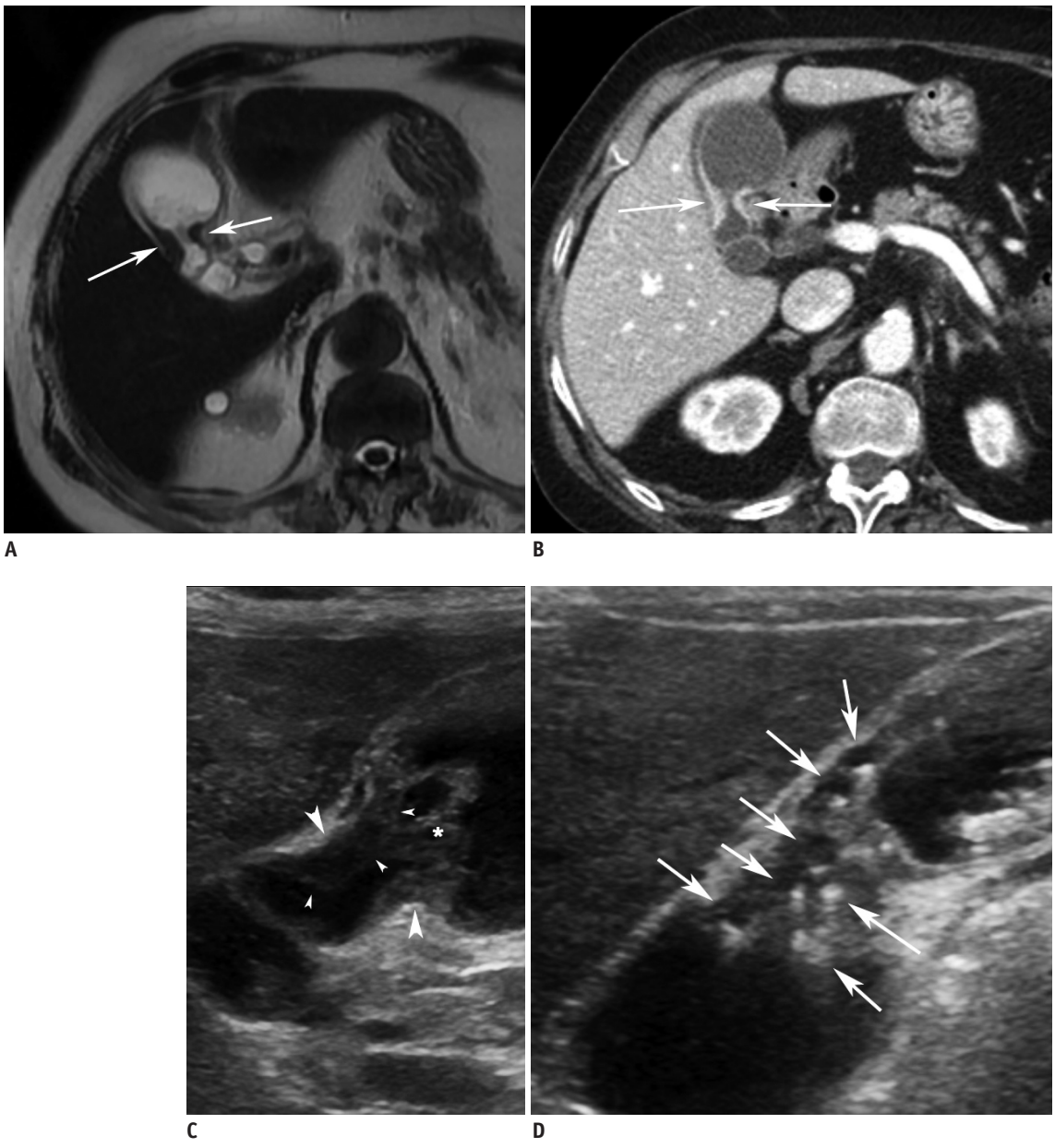

Fig. 2. Gallbladder body cancer (pT2) in 81-year-old female.
A. MR image with T2-weighted single-shot fast spin-echo sequence shows segmental thickening (arrows) without evidence of intramural cysts at body of gallbladder. **B.** CT image during portal venous phase shows segmental wall thickening with strong contrast enhancement at body (arrows). **C.** High-resolution ultrasound image showing segmental wall thickening (arrowheads) without evidence of intramural cysts or intramural echogenic material deposition at body. Asterisks (*) indicate sludge. **D.** High-resolution ultrasound image in patient with segmental adenomyomatosis shows multiple cysts and echogenic materials (arrows) within thickened walls. This image clearly shows difference between adenomyomatosis and cancer on ultrasound image.

A p value of less than 0.05 was considered a statistically significant difference.

RESULTS

For both reviewers, the Az values and ROC curves of the three modalities in the differential diagnosis of ADM and GB cancer are shown in Table 1. No significant difference was found in the Az values among the three modalities for each reviewer ($p > 0.05$). Furthermore, no significant difference was found in the Az values for each imaging modality between the two reviewers ($p > 0.05$). However, for reviewer 2 with less experience in abdominal radiology, the p value for the Az comparison between HRUS and CT was near 0.05 ($p = 0.051$). The interobserver agreement (κ values) between the two reviewers were 0.78, 0.66, and 0.64 for HRUS,

Korean Journal of Radiology
KJR

CT, and MRI, respectively, representing good to excellent agreement.

For both reviewers, the sensitivity, specificity and accuracy of the three modalities are shown in Table 2 and Figure 3. The mean sensitivity of MRI with MRCP (80.8%) was significantly superior to that of MDCT (50.0%) (p = 0.0215). However, the mean sensitivity of MRI with MRCP (80.8%) was not significantly different from that of HRUS (73.1%) (p > 0.05). MDCT showed the lowest mean sensitivity (50.0%). However, the difference between HRUS and MDCT was not significant for the mean sensitivity (p > 0.05). The mean specificities among the three modalities were not significantly different (p > 0.05).

Table 1. The Az Values of High-Resolution Ultrasound (HRUS), CT, and MR Imaging (MRI) for Diagnosis of Adenomyomatosis by Two Reviewers

	Az Value		*P**
Reviewer 1			
HRUS	0.936 (0.811–0.989)	vs. CT	0.734
		vs. MRI	0.832
CT	0.957 (0.841–0.996)	vs. MRI	0.360
MRI	0.920 (0.790–0.982)		
Reviewer 2			
HRUS	0.981 (0.879–1.000)	vs. CT	0.051
		vs. MRI	0.506
CT	0.840 (0.690–0.937)	vs. MRI	0.084
MRI	0.950 (0.831–0.994)		
Mean			
HRUS	0.959 (0.889–0.990)	vs. CT	0.226
		vs. MRI	0.582
CT	0.898 (0.810–0.954)	vs. MRI	0.454
MRI	0.935 (0.857–0.978)		

Note.— Data in parentheses represent 95% confidence intervals. *Paired Z-test for paired data.

DISCUSSION

The diagnostic performance of HRUS for the differentiation of ADM from GB cancer was comparable with MRI with MRCP. In a previously published study, the diagnostic performance of conventional US was inferior to CT and MRI with the half-Fourier RARE technique in diagnosing the ADM (7). However, the present study showed that the diagnostic performance of HRUS was equivalent to that of MRI for differentiating ADM from GB cancer. The improvement in diagnostic performance of US is most likely the result of the technological advances which have been utilized since 2000, such as harmonics, compounding techniques, and speckle reduction.

The demonstration of an intramural cyst within a

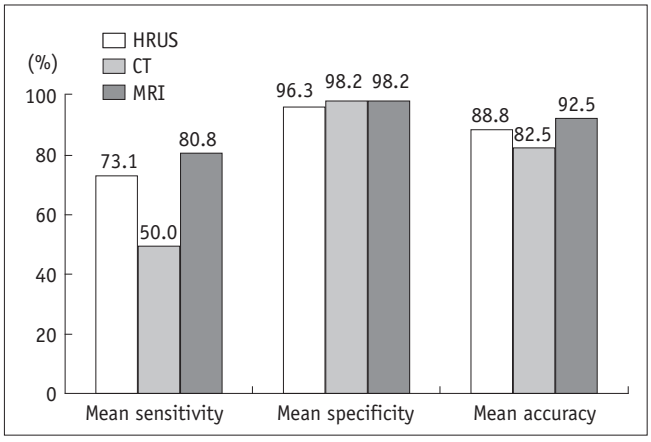

Fig. 3. Bar graph displaying mean sensitivities, specificities, and accuracies of high-resolution ultrasound (HRUS), CT, and MRI for diagnosis of adenomyomatosis of gallbladder.

Table 2. Sensitivity, Specificity, and Accuracy of High-Resolution Ultrasound (HRUS), CT, and MR Imaging (MRI)

	Sensitivity (%)	Specificity (%)	Accuracy (%)
Reviewer 1			
HRUS	69.2 (38.6–90.9)	96.3 (81.0–99.9)	87.5 (73.2–95.8)
CT	46.2 (19.2–74.9)	100.0 (54.1–100.0)	82.5 (67.2–92.7)
MRI	76.9 (46.2–85.0)	100.0 (69.2–100.0)	92.5 (79.6–98.4)
Reviewer 2			
HRUS	76.9 (46.2–95.0)	96.3 (81.0–99.9)	90.0 (76.3–97.2)
CT	53.9 (25.1–80.8)	96.3 (81.0–99.9)	82.5 (67.2–92.7)
MRI	84.6 (54.6–98.1)	96.3 (81.0–99.9)	92.5 (79.6–98.4)
Mean			
HRUS	73.1 (52.2–88.4)	96.3 (87.3–99.5)	88.8 (79.7–94.7)
CT	50.0 (29.9–70.1)*	98.2 (90.1–100.0)	82.5 (72.4–90.1)
MRI	80.8 (60.6–93.4)*	98.2 (90.1–100.0)	92.5 (84.4–97.2)

Note.— Data in parentheses represent 95% confidence intervals. *There is statistically significant difference in mean sensitivity between CT and MRI (p = 0.0215).

thickened GB wall (Rokitansky-Aschoff sinus) is very critical because it is a pathognomonic imaging finding for diagnosing ADM (Fig. 4) (26). To demonstrate the presence of a cyst or cystic portion in a lesion, US and MRI are known to be better than CT, especially when the cyst is small (6, 8, 10, 21-23). The demonstration of cystic lesions is enhanced by higher frequency, harmonics and compounding techniques (10).

In addition, the demonstration of cholesterol crystals or stones deposited in the Rokitansky-Aschoff sinuses is also very important for the diagnosis of ADM (Fig. 5). In this regard, US has advantages over MRI and CT because these deposits are observed as very bright, with a comet-tail artifact and/or color-Doppler twinkling artifact on US. The depiction of these materials is enhanced with the use of higher frequency, harmonics, compounding techniques and speckle reduction due to the higher spatial and contrast resolution and reduction of noise and artifacts (27, 28).

Haradome et al. (23) reported in 2003 that the mean Az value for MR imaging with MRCP in differentiating between adenomyomatosis and GB cancer was 0.93 ± 0.03. The present study showed that the mean Az value for MR imaging with MRCP was 0.935 (95% confidence intervals, 0.857–0.978), which matches the result of Haradome et al.'s

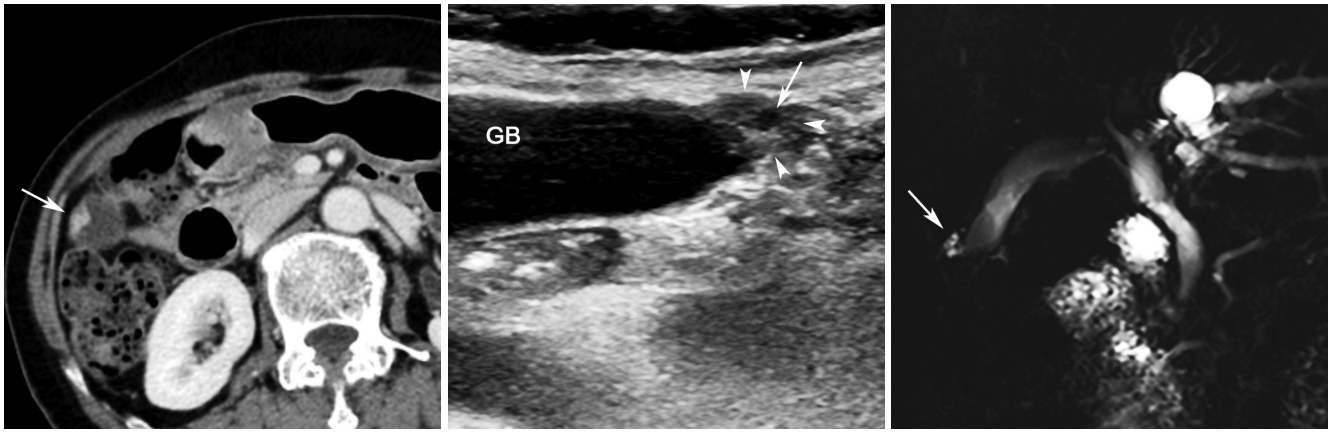

Fig. 4. Fundal adenomyoma in 72-year-old female.
A. CT image during portal venous phase showing focal wall thickening with heterogeneous contrast enhancement (arrow) at fundus of GB. **B.** High-resolution ultrasound image showing focal thickening at fundus (arrowheads) containing cystic lesion (arrow), indicating presence of dilated intramural Rokitansky-Aschoff sinuses. **C.** MR image with thick-slab, T2-weighted fast spin-echo sequence demonstrating focal high signal intensity lesion (arrow), indicating presence of dilated intramural Rokitansky-Aschoff sinuses at fundus. GB = gallbladder

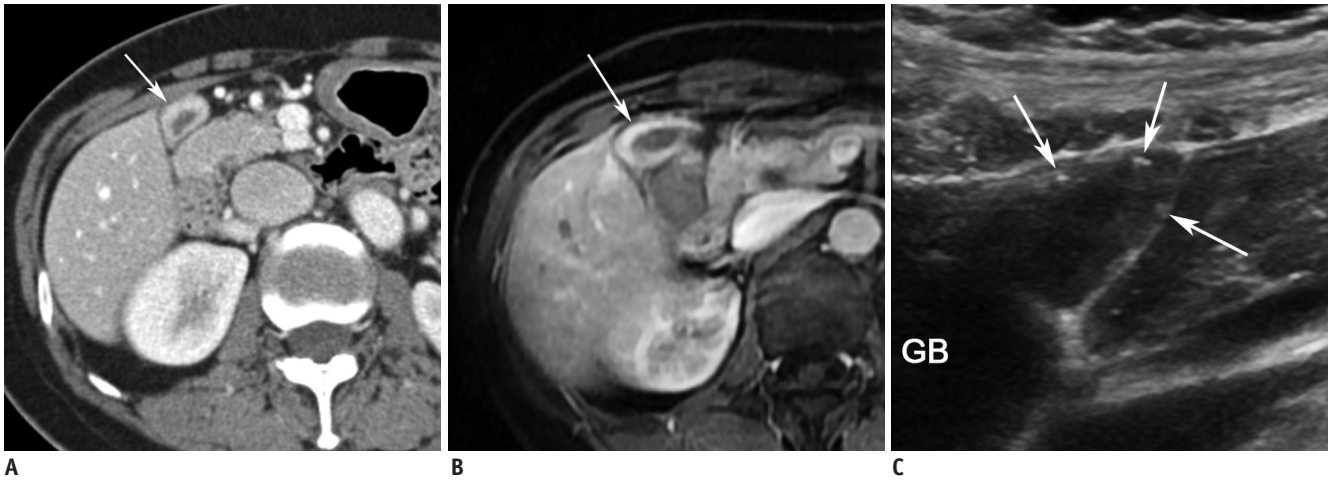

Fig. 5. Adenomyomatosis in GB fundus in 61-year-old female.
A. CT image during portal venous phase showing marked wall thickening with strong contrast enhancement (arrow) at fundus of GB. There is no evidence of intramural cysts. **B.** T1-weighted MR image during portal venous phase also shows diffuse thickening at fundus with strong contrast enhancement (arrow). There is no evidence of intramural cysts on T2-weighted images (not shown). **C.** High-resolution ultrasound image shows diffuse wall thickening at fundus with multiple intramural deposition of echogenic materials (arrows) which represent intramural cholesterol crystal deposition. This finding favors diagnosis of adenomyomatosis more than GB cancer. GB = gallbladder

Korean Journal of Radiology
KJR

study.

In 2007, Ching et al. (6) reported the diagnostic performance of CT for the differentiation between ADM and GB cancer with a sensitivity of 30% and a specificity of 93%. In the present study, one of the main reasons for the superior values of the diagnostic performance of CT (sensitivity 50.0%, specificity 98.2%) could be that a 2.5–3.2-mm slice thickness was used for all patients whereas a 5-mm or thicker slice thickness was used in 94% of the patients in Ching et al.'s study.

For the evaluation of GB lesions in the clinical practice, HRUS offers economic efficiency and comfortable exam conditions compared to other imaging modalities, such as CT, MRI, and endoscopic ultrasonography. In addition, HRUS could become an important diagnostic modality for the differential diagnosis and staging of GB polypoid lesions and early GB cancer (11).

The present study has several limitations. First, this study excluded other diseases, such as xanthogranulomatous cholecystitis or chronic cholecystitis, which also show GB wall thickening. In addition, the readers were aware that the diagnosis was either ADM or GB cancer. Therefore the diagnostic performance of HRUS could be potentially overestimated. However, this study focused on revisiting the diagnostic performance of US for the differentiation between ADM and GB cancer, like as in a study which was published in 2001 (7). Second, this study is more likely to include more complicated cases of ADM than the cases encountered in real clinical practice. ADM is surgically proven and full imaging studies including HRUS, CT, and MRI with MRCP are performed only when patients have clinical symptoms or if there are difficulties in the differentiation of ADM from GB cancer in the imaging studies. This explains also why a small number of patients with ADM were included in this study only, even though a 6-year inclusion period was given. In the daily clinical practice, there are much larger numbers of typical ADM which can be confidently diagnosed by imaging alone without a need for surgery. Third, the morbid obesity is a significant obstacle to US. Consequently, the diagnostic performance of HRUS can vary according to the prevalence of morbid obesity in each country (29). Last, HRUS has operator-dependent and anatomical limitations. To perform HRUS correctly, sufficient experience with HRUS and a deep understanding of HRUS findings in various GB diseases are required. HRUS can be limited in evaluating the GB neck in obese patients and in evaluating the GB fundus in patients whose overlying abdominal walls are generating significant reverberation artifacts, which may lead to misdiagnosis.

In conclusion, HRUS seems to have a diagnostic performance that is comparable with MRI with MRCP, and MDCT may have the lowest sensitivity and accuracy for the differentiation of ADM from GB cancer.

REFERENCES

1. Jutras JA. Hyperplastic cholecystoses; Hickey lecture, 1960. *Am J Roentgenol Radium Ther Nucl Med* 1960;83:795-827
2. Colquhoun J. Adenomyomatosis of the gall-bladder (intramural diverticulosis). *Br J Radiol* 1961;34:101-112
3. Fotopoulos JP, Crampton AR. Adenomyomatosis of the gallbladder. *Med Clin North Am* 1964;48:9-36
4. Williams I, Slavin G, Cox A, Simpson P, de Lacey G. Diverticular disease (adenomyomatosis) of the gallbladder: a radiological-pathological survey. *Br J Radiol* 1986;59:29-34
5. Gerard PS, Berman D, Zafaranloo S. CT and ultrasound of gallbladder adenomyomatosis mimicking carcinoma. *J Comput Assist Tomogr* 1990;14:490-491
6. Ching BH, Yeh BM, Westphalen AC, Joe BN, Qayyum A, Coakley FV. CT differentiation of adenomyomatosis and gallbladder cancer. *AJR Am J Roentgenol* 2007;189:62-66
7. Yoshimitsu K, Honda H, Aibe H, Shinozaki K, Kuroiwa T, Irie H, et al. Radiologic diagnosis of adenomyomatosis of the gallbladder: comparative study among MRI, helical CT, and transabdominal US. *J Comput Assist Tomogr* 2001;25:843-850
8. Oktar SO, Yücel C, Ozdemir H, Ulutürk A, Işik S. Comparison of conventional sonography, real-time compound sonography, tissue harmonic sonography, and tissue harmonic compound sonography of abdominal and pelvic lesions. *AJR Am J Roentgenol* 2003;181:1341-1347
9. Dahl JJ, Soo MS, Trahey GE. Clinical evaluation of combined spatial compounding and adaptive imaging in breast tissue. *Ultrason Imaging* 2004;26:203-216
10. Yen CL, Jeng CM, Yang SS. The benefits of comparing conventional sonography, real-time spatial compound sonography, tissue harmonic sonography, and tissue harmonic compound sonography of hepatic lesions. *Clin Imaging* 2008;32:11-15
11. Jang JY, Kim SW, Lee SE, Hwang DW, Kim EJ, Lee JY, et al. Differential diagnostic and staging accuracies of high resolution ultrasonography, endoscopic ultrasonography, and multidetector computed tomography for gallbladder polypoid lesions and gallbladder cancer. *Ann Surg* 2009;250:943-949
12. Yoon SH, Lee JM, So YH, Hong SH, Kim SJ, Han JK, et al. Multiphasic MDCT enhancement pattern of hepatocellular carcinoma smaller than 3 cm in diameter: tumor size and cellular differentiation. *AJR Am J Roentgenol* 2009;193:W482-W489
13. Rice J, Sauerbrei EE, Semogas P, Cooperberg PL, Burhenne HJ. Sonographic appearance of adenomyomatosis of the

gallbladder. *J Clin Ultrasound* 1981;9:336-337
14. Raghavendra BN, Subramanyam BR, Balthazar EJ, Horii SC, Megibow AJ, Hilton S. Sonography of adenomyomatosis of the gallbladder: radiologic-pathologic correlation. *Radiology* 1983;146:747-752
15. Brambs HJ, Wrazidlo W, Schilling H. [The sonographic image of gallbladder adenomyomatosis]. *Rofo* 1990;153:633-636
16. Hwang JI, Chou YH, Tsay SH, Chiang JH, Chang CY, Boland GW, et al. Radiologic and pathologic correlation of adenomyomatosis of the gallbladder. *Abdom Imaging* 1998;23:73-77
17. Boscak AR, Al-Hawary M, Ramsburgh SR. Best cases from the AFIP: adenomyomatosis of the gallbladder. *Radiographics* 2006;26:941-946
18. Clouston JE, Thorpe RJ. Case report--CT findings in adenomyomatosis of the gallbladder. *Australas Radiol* 1991;35:86-87
19. Chao C, Hsiao HC, Wu CS, Wang KC. Computed tomographic finding in adenomyomatosis of the gallbladder. *J Formos Med Assoc* 1992;91:467-469
20. Stunell H, Buckley O, Geoghegan T, O'Brien J, Ward E, Torreggiani W. Imaging of adenomyomatosis of the gall bladder. *J Med Imaging Radiat Oncol* 2008;52:109-117
21. Miyazaki T, Yamashita Y, Tsuchigame T, Yamamoto H, Urata J, Takahashi M. MR cholangiopancreatography using HASTE (half-Fourier acquisition single-shot turbo spin-echo) sequences. *AJR Am J Roentgenol* 1996;166:1297-1303
22. Yoshimitsu K, Honda H, Jimi M, Kuroiwa T, Hanada K, Irie H, et al. MR diagnosis of adenomyomatosis of the gallbladder and differentiation from gallbladder carcinoma: importance of showing Rokitansky-Aschoff sinuses. *AJR Am J Roentgenol* 1999;172:1535-1540
23. Haradome H, Ichikawa T, Sou H, Yoshikawa T, Nakamura A, Araki T, et al. The pearl necklace sign: an imaging sign of adenomyomatosis of the gallbladder at MR cholangiopancreatography. *Radiology* 2003;227:80-88
24. Levy AD, Murakata LA, Rohrmann CA Jr. Gallbladder carcinoma: radiologic-pathologic correlation. *Radiographics* 2001;21:295-314; questionnaire, 549-555
25. Metz CE. Some practical issues of experimental design and data analysis in radiological ROC studies. *Invest Radiol* 1989;24:234-245
26. Gore RM, Yaghmai V, Newmark GM, Berlin JW, Miller FH. Imaging benign and malignant disease of the gallbladder. *Radiol Clin North Am* 2002;40:1307-1323, vi
27. Lee JY, Choi BI, Han JK, Lee JM, Kim SH, Choi JY, et al. High resolution ultrasonographic evaluation of the gallbladder: value of advanced imaging techniques. *J Korean Soc Ultrasound Med* 2005;24:169-175
28. Liasis N, Klonaris C, Katsargyris A, Georgopoulos S, Labropoulos N, Tsigris C, et al. The use of Speckle Reduction Imaging (SRI) Ultrasound in the characterization of carotid artery plaques. *Eur J Radiol* 2008;65:427-433
29. Oria HE. Pitfalls in the diagnosis of gallbladder disease in clinically severe obesity. *Obes Surg* 1998;8:444-451